Journal of Computational Physics 284 (2015) 631–647

Contents lists available at ScienceDirect

Journal of Computational Physics

www.elsevier.com/locate/jcp

A revised scheme to compute horizontal covariances in an oceanographic 3D-VAR assimilation system

R. Farina [a,*], S. Dobricic [b,1], A. Storto [b], S. Masina [b], S. Cuomo [c,2]

[a] Inst. for High-Performance Comput. and Networking, Nat. Res. Council (ICAR-CNR), Via Pietro Castellino 111, Naples, 80131, Italy
[b] Centro Euro–Mediterraneo sui Cambiamenti Climatici, Viale Aldo Moro 44, Bologna, Italy
[c] Department of Mathematics and Applications, University of Naples Federico II, Via Cinthia, 80126, Naples, Italy

ARTICLE INFO

Article history:
Received 13 October 2014
Received in revised form 30 December 2014
Accepted 2 January 2015
Available online 9 January 2015

Keywords:
Data assimilation
Recursive Gaussian filter and numerical optimization

ABSTRACT

We propose an improvement of an oceanographic three dimensional variational assimilation scheme (3D-VAR), named OceanVar, by introducing a recursive filter (RF) with the third order of accuracy (3rd-RF), instead of an RF with first order of accuracy (1st-RF), to approximate horizontal Gaussian covariances. An advantage of the proposed scheme is that the CPU's time can be substantially reduced with benefits on the large scale applications. Experiments estimating the impact of 3rd-RF are performed by assimilating oceanographic data in two realistic oceanographic applications. The results evince benefits in terms of assimilation process computational time, accuracy of the Gaussian correlation modeling, and show that the 3rd-RF is a suitable tool for operational data assimilation.

1. Introduction

Ocean data assimilation is a crucial task in operational oceanography, responsible for optimally combining observational measurements and a prior knowledge of the state of the ocean in order to provide initial conditions for the forecast model. How the informative content of the observations is spread horizontally in space depends on the operator used to model horizontal covariances. The three-dimensional variational data assimilation scheme called OceanVar [10] represents horizontal covariances of background errors in temperature and salinity by approximate Gaussian functions that depend only on the horizontal distance between two model points. Gaussian background error term has a positive impact on convergence of minimization of variational methods for incomplete and noisy observations in space dimension as shown by Navon et al. [19]. In the framework of optimal interpolation, where the analysis is found by using only the nearest observations, the calculation of the Gaussian function can be made directly from the distances between the model point and the typically small number of nearby observations. This kind of solution may be impractical in the variational framework, where it is necessary to calculate the covariances between each pair of model points in the horizontal. Instead, variational schemes often use linear operators that approximate the Gaussian function (e.g., [29]).

* Corresponding author. Tel.: +39 6139520.
E-mail addresses: raffaele.farina@na.icar.cnr.it (R. Farina), srdan.dobricic@jrc.ec.europa.eu (S. Dobricic), salvatore.cuomo@unina.it (S. Cuomo).
[1] Tel.: +39 051 378267.
[2] Tel.: +39 081675624.

http://dx.doi.org/10.1016/j.jcp.2015.01.003
0021-9991/

Fast mathematical tools for simulating the action of Gaussian correlation, to achieve acceptably isotropic covariance functions, are recursive Gaussian filters (RFs) and diffusion equation. In meteorology, Lorenc [16] approximated the Gaussian function by applying one-dimensional recursive filters (RF) with the first-order accuracy successively in the two perpendicular directions. In oceanography, Weaver et al. [30] used the explicit integration of the two-dimensional diffusion equation. Purser et al. [23] developed higher order recursive filters for use in atmospheric models. The OceanVar scheme described in [10] used the RF of the first order (1st-RF) with imaginary sea points for the processing on the coast. Mirouze and Weaver [18] implemented the implicit integration of one-dimensional diffusion equations.

Successive applications of one-dimensional recursive filters or implicit integrations of the diffusion equation in the two perpendicular directions are much more computationally efficient than the explicit integration of the diffusion equation [18]. First order accurate operators used in most of these schemes still require several iterations to approximate the Gaussian function. For example, the 1st-RF in OceanVar generally applies 5 iterations and is the most computationally demanding part.

Recursive filters with higher order accuracy require more operations for each iteration, but only one iteration might be enough to accurately approximate the Gaussian function. Generally high order recursive filters can be obtained by means of different strategies e.g. in [9,23,24,31]. The main difference among them is the mathematical methodology used to obtain the filter coefficients. In meteorology, Purser et al. [23] resolve an inverse problem with exponential matrix of finite differences operator approximating the second derivative d^2/dx^2 on a line grid of uniform spacing Δx. They use truncated Taylor expansion to approximate the exponential matrix and obtain the filter coefficients through the LL^T factorization of the resulting filtering model. The degree of the Taylor polynomial is the order of RF obtained.

In this study, we develop an RF of third order accuracy (3rd-RF), still with the use of the imaginary points for treatment on the coast, that needs only one iteration to approximate the Gaussian function and allows different length-scales. Our approach, based on Young and Van Vliet [31], determines the filter coefficients of a 3rd-RF by the matrix–vector multiplication of Gaussian operator for an input field, using a known rational approximation of the Gaussian function. Note that this strategy has been so far exploited only in signal processing, and represents a completely novel methodology in geophysical data assimilation. Furthermore, we compare the 3rd-RF performance with those of the existing 1st-RF on two different configurations of OceanVar: Mediterranean Sea and Global Ocean. The new filter should be at least as accurate as the existing one and it should execute more rapidly on massively parallel computers. Tests on parallel computer architectures are especially important because higher order accurate filters compute the solution from several nearby points, and as a consequence, transfer more data among processors eventually becoming less efficient.

Section 2 gives a general description of the existing OceanVar data assimilation scheme. Section 3 demonstrates in detail the development of the 3rd-RF. It also provides all numerical values and the method to compute the coefficients of the filter with different length-scales. Moreover, we give an estimate of the approximation error between the result of an RF and an actual Gaussian convolution. In Sections 4 and 5, the filter is applied in the operational version of OceanVar used respectively in the Mediterranean Sea [21] and Global Ocean [27]. Its performance is compared to that of the 1st-RF. In Section 6 we present conclusions and indicate the future directions of the development of the operator for the horizontal covariances.

2. General description

2.1. The OceanVar computational kernel

The computational kernel of the OceanVar data assimilation scheme is based on the minimization of the following cost function:

$$J(\mathbf{x}) = \frac{1}{2}\|\mathbf{x}-\mathbf{x_b}\|^2_{\mathbf{B}^{-1}} + \frac{1}{2}\|\mathbf{y}-H(\mathbf{x})\|^2_{\mathbf{R}^{-1}} \tag{1}$$

In Eq. (1) the vector $\mathbf{x} = [\mathbf{T}, \mathbf{S}, \boldsymbol{\eta}, \mathbf{u}, \mathbf{v}]^\top$ is an ocean state vector composed by the temperature $\mathbf{T}$, the salinity $\mathbf{S}$, sea level $\boldsymbol{\eta}$ and horizontal velocity field $(\mathbf{u}, \mathbf{v})$. The vector $\mathbf{x_b}$ is the background state vector, obtained by numerical solution of an ocean forecasting model and is an approximation of the "true" state vector $\mathbf{x_t}$. The difference between background $\mathbf{x_b}$ and any state vector $\mathbf{x}$ is denoted by $\boldsymbol{\delta}\mathbf{x}$:

$$\mathbf{x_b} = \mathbf{x} + \boldsymbol{\delta}\mathbf{x} \tag{2}$$

The vectors $\mathbf{x}$ and $\mathbf{x_b}$ are defined on the same space called *physical space*. The vector $\mathbf{y}$ in (1) is the observational vector defined on a different space called *observational space* and the function H is a non-linear operator that converts values defined in physical space to values defined in observational space. An ocean state vector $\mathbf{x}$ is related to observations $\mathbf{y}$ by means the following relation:

$$\mathbf{y} = H(\mathbf{x}) + \boldsymbol{\delta}\mathbf{y} \tag{3}$$

where $\boldsymbol{\delta}\mathbf{y}$ is the misfit between the observation vector and its model counterpart (the residual in the observation term of the cost function). In (1) the matrix $\mathbf{R} = \langle \boldsymbol{\delta}\mathbf{y_t}\ \boldsymbol{\delta}\mathbf{y_t}^\top \rangle$, with $\boldsymbol{\delta}\mathbf{y_t} = \mathbf{y} - H(\mathbf{x_t})$, is the observational error covariance matrix and it

is assumed generally to be diagonal, i.e. observational errors are seen as statistically independent. The $\mathbf{B} = \langle \boldsymbol{\delta}\mathbf{x_t}\ \boldsymbol{\delta}\mathbf{x_t}^{\top} \rangle$, with $\boldsymbol{\delta}\mathbf{x_t} = \mathbf{x_b} - \mathbf{x_t}$, is the background error covariance matrix and is never assumed to be diagonal in its representation.

Problem (1) is solved by minimizing the following explicit form of the cost function $J(\mathbf{x})$:

$$J(\mathbf{x}) = \frac{1}{2}(\mathbf{x} - \mathbf{x_b})^{\top}\mathbf{B}^{-1}(\mathbf{x} - \mathbf{x_b}) + \frac{1}{2}\big(\mathbf{y} - H(\mathbf{x})\big)^{\top}\mathbf{R}^{-1}\big(\mathbf{y} - H(\mathbf{x})\big). \tag{4}$$

It is often numerically convenient to exploit the weak non-linearity of H by approximating $H(\mathbf{x})$, for small increments $\boldsymbol{\delta}\mathbf{x}$, with a linear approximation around the background vector $\mathbf{x_b}$:

$$H(\mathbf{x}) \approx H(\mathbf{x_b}) + \mathbf{H}\boldsymbol{\delta}\mathbf{x}. \tag{5}$$

where the linear operator $\mathbf{H}$ is the H's Jacobian evaluated at $\mathbf{x} = \mathbf{x_b}$.

The cost function J, using (5), is approximated by the following quadratic function:

$$J(\boldsymbol{\delta}\mathbf{x}) = \frac{1}{2}\boldsymbol{\delta}\mathbf{x}^{\top}\mathbf{B}^{-1}\boldsymbol{\delta}\mathbf{x} + \frac{1}{2}(\mathbf{d} - \mathbf{H}\boldsymbol{\delta}\mathbf{x})^{\top}\mathbf{R}^{-1}(\mathbf{d} - \mathbf{H}\boldsymbol{\delta}\mathbf{x}) \tag{6}$$

defined on increment space. In (6) the vector $\mathbf{d} = \mathbf{y} - H(\mathbf{x_b})$ is the innovation (or misfit).

The minimum of the cost function $J(\boldsymbol{\delta}\mathbf{x})$ on the increment space may be justified by posing $\nabla J(\boldsymbol{\delta}\mathbf{x}) = 0$. Then we obtain, as also shown in [15], the following preconditioned linear system:

$$\big(\mathbf{I} + \mathbf{B}\mathbf{H}^{\mathbf{T}}\mathbf{R}^{-1}\mathbf{H}\big)\boldsymbol{\delta}\mathbf{x} = \mathbf{B}\mathbf{H}^{\mathbf{T}}\mathbf{R}^{-1}\mathbf{d} \tag{7}$$

To solve the linear equation system (7) iterative methods able to converge toward a practical solution are needed. OceanVar uses the limited-memory Broyden–Fletcher–Goldfarb–Shanno (L-BFGS) [4]. However the choice of minimizer depends on the possibility to include in Eq. (6) weakly or not smooth terms. For large-scale non-smooth terms in the cost function, a novel solution is represented by the limited-memory bundle method (LMBM) shown by Steward et al. [26].

Both minimizers make for each iteration the matrix–vector operation of some vector $\mathbf{v} = (\mathbf{H}^{\mathbf{T}}\mathbf{R}^{-\mathbf{1}}\mathbf{H})\boldsymbol{\delta}\mathbf{x}$ with the covariance matrix $\mathbf{B}$. This computational kernel is required at each iteration, and its huge computational complexity is a bottleneck in practical data assimilation. This problem can be overcome by decomposing the covariance matrix $\mathbf{B}$ in the following form:

$$\mathbf{B} = \mathbf{V}\mathbf{V}^{T} \tag{8}$$

However due to its still large size, the matrix $\mathbf{V}$ is split at each minimization iteration as a sequence of linear operators [30]. More precisely, in OceanVar the matrix $\mathbf{V}$ is decomposed as:

$$\mathbf{V} = \mathbf{V}_D\mathbf{V}_{uv}\mathbf{V}_{\eta}\mathbf{V}_H\mathbf{V}_V \tag{9}$$

where the linear operator $\mathbf{V}_V$ transforms coefficients which multiply vertical EOFs into vertical profiles of temperature and salinity defined at the model vertical levels, $\mathbf{V}_H$ applies the Gaussian filtering to the fields of temperature, salinity and sea surface height. $\mathbf{V}_{\eta}$ applies a barotropic model for the computation of the sea surface height. $\mathbf{V}_{uv}$ calculates velocity from sea surface height, temperature and salinity, and $\mathbf{V}_D$ applies a divergence damping filter on the velocity field. A more detailed formulation of each linear operator is described in Dobricic and Pinardi [10]. In this paper we focus on the operator $\mathbf{V}_H$.

2.2. OceanVar horizontal covariances

The OceanVar horizontal error covariances matrix $\mathbf{V}_H$ is assumed to be a Gaussian matrix [10]. In oceanographic models, isotropic and Gaussian spatial correlations can be relatively efficiently approximated by an iterative application of a Gaussian RF [14,16] that requires only a few steps. Moreover, its application on a horizontal grid can be split into two independent directions [23]. We highlight that the ocean recursive filter scheme is more complicated than the atmospheric case due to the presence of coastlines. In this framework, the horizontal error covariances $\mathbf{V}_H$ is factored as:

$$\mathbf{V}_H = \mathbf{G_y}\mathbf{G_x} \tag{10}$$

where $\mathbf{G_x}$ and $\mathbf{G_y}$ represent the Gaussian operators in directions x and y.

In the next section, we present an optimally revised RF to compute an approximation of the image of the temperature and salinity fields by means of matrices $\mathbf{G_x}$ and $\mathbf{G_y}$.

3. Recursive filters for a 3D-VAR assimilation scheme

Because of the separability of the two-dimensional (2D) Gaussian function (that is $e^{-(x^2+y^2)} = e^{-x^2}e^{-y^2}$), a 2D-RF can be obtained applying a 1D-RF on each row and column of the discrete domain (e.g., [20]). Then we will consider the properties of the RFs only on the one dimensional case.

In particular, the application of a one-dimensional n-th order RF on a grid of m points requires two main steps:

$$p_i^k = \beta s_i^{k-1} + \sum_{j=1}^{n} \alpha_j p_{i-j}^k \quad i = n+1, m:+1,\ k = 1, 2, \ldots, K \tag{11}$$

$$s_i^k = \beta p_i^k + \sum_{j=1}^{n} \alpha_j s_{i+j}^k \quad i = m, n+1:-1,\ k = 1, 2, \ldots, K \tag{12}$$

where K is the total filter iterations number, s^0 is the input distribution, p^k is the k-th output vector of the forward procedure (11) and s^k is the k-th output vector of the backward procedure (12), corresponding to the input distribution for the $(k+1)$-th forward procedure. Finally, $\alpha_j,\ j = 1, 2, ..., n$ and β are the filter smoothing coefficients.

3.1. The 1st-RF and 3rd-RF in OceanVar

In the previous OceanVar scheme, the 1st-RF algorithm of Hayden and Purser [14], Purser et al. [23] was implemented along the x and y directions. For the treatment at the boundaries, it is used the strategy of the imaginary sea points described by Dobricic and Pinardi [10]. The revised scheme uses a 3rd-RF based on the works of Young and Van Vliet [31], Van Vliet et al. [28] and uses the same boundary conditions of the 1st-RF. OceanVar model computes for each grid point the filter coefficients that depend on the correlation radius $R(x, y)$ and the grid distances Δx and Δy. Then OceanVar allows the use of different length-scales σ for the Gaussian covariance functions.

The one dimensional 1st-RF version, implemented in OceanVar, is composed by the following rules:

$$p_1^k = \beta_1 s_1^{k-1}, \quad k = 1, 2, ..., K \tag{13}$$

$$p_i^k = \beta_i s_i^{k-1} + \alpha_i p_{i-1}^k \quad i = 2, m:+1,\ k = 1, 2, \ldots, K \tag{14}$$

$$s_m^k = \beta_m p_m^k, \quad k = 1, 2, \ldots, K \tag{15}$$

$$s_i^k = \beta_i p_i^k + \alpha_i s_{i+1}^k \quad i = m-1, 2:-1,\ k = 1, 2, \ldots, K \tag{16}$$

where the parameter $\alpha_i, \beta_i \in (0, 1)$ and $\beta_i = (1 - \alpha_i)$ are the filter coefficients at the i-th grid point. In order to obtain the filter smoothing coefficients α_i and β_i, the crucial relationship in Hayden and Purser [14]:

$$R_i^2 = 2K \frac{\alpha_i}{(1-\alpha_i)^2} \Delta x_i^2 \tag{17}$$

is considered. R_i and Δx_i are respectively the correlation radius and the grid distance at the i-th grid point. By means of Eq. (17), it follows that:

$$(1-\alpha_i)^2 = 2K\left(\Delta x_i^2 / R_i^2\right) - 2K\left(\Delta x_i^2 / R_i^2\right)(1-\alpha_i). \tag{18}$$

Calculating the roots $\beta_i = (1 - \alpha_i)$ from Eq. (18), we obtain that α_i and β_i are:

$$\begin{aligned} \alpha_i &= 1 + \frac{K\Delta x_i^2}{R_i^2} - \sqrt{\frac{K\Delta x_i^2}{R_i^2}\left(\frac{K\Delta x_i^2}{R_i^2} + 2\right)} \\ \beta_i &= -\frac{K\Delta x_i^2}{R_i^2} + \sqrt{\frac{K\Delta x_i^2}{R_i^2}\left(\frac{K\Delta x_i^2}{R_i^2} + 2\right)} \end{aligned} \tag{19}$$

In the following, we are considering a 3rd-RF that approximates quite successfully in just one iteration the Gaussian convolution considered in Mirouze and Weaver [18] and that allows different length-scales for each grid point of the computational domain. It is based on the works of Young and Van Vliet [31] and Van Vliet et al. [28] and is widely used for the blurring problems in digital image but not in geophysical data assimilation.

In the next remark we are presenting a simple and accurate adapted version of a 3rd-RF for OceanVar scheme applied to a one-dimensional grid. The procedure to obtain the 3rd-RF coefficients is given in Appendix A in Theorem 1 for the simple case of the spatially homogeneous length-scales σ.

Remark 1. For each i-th grid point of a finite one-dimensional grid with correlation radius R_i and grid spacing Δx_i, a normalized 3rd-RF is given by:

$$p_i = \beta_i s_i^0 + \alpha_{i,1} p_{i-1} + \alpha_{i,2} p_{i-2} + \alpha_{i,3} p_{i-3} \quad i = 4, m\ :+1 \tag{20}$$

$$s_i = \beta_i p_i + \alpha_{i,1} s_{i+1} + \alpha_{i,2} s_{i+2} + \alpha_{i,3} s_{i+3}. \quad i = m-3, 1\ :-1. \tag{21}$$

where the function s_i^0 is the input distribution, $\alpha_{i,1} = a_{i,1}/a_{i,0}$, $\alpha_{i,2} = a_{i,2}/a_{i,0}$, $\alpha_{i,3} = a_{i,3}/a_{i,0}$ and $\beta_i = \sqrt[4]{2\pi (R_i/\Delta x_i)^2}(1 - (\alpha_{i,1} + \alpha_{i,2} + \alpha_{i,3}))$ are the filtering coefficients and:

$$a_{i,0} = 3.738128 + 5.788982\left(\frac{R_i}{\Delta x_i}\right) + 3.382473\left(\frac{R_i}{\Delta x_i}\right)^2 + 1.\left(\frac{R_i}{\Delta x_i}\right)^3$$
$$a_{i,1} = 5.788982\left(\frac{R_i}{\Delta x_i}\right) + 6.764946\left(\frac{R_i}{\Delta x_i}\right)^2 + 3.\left(\frac{R_i}{\Delta x_i}\right)^3$$
$$a_{i,2} = -3.382473\left(\frac{R_i}{\Delta x_i}\right)^2 - 3.\left(\frac{R_i}{\Delta x_i}\right)^3$$
$$a_{i,3} = 1.\left(\frac{R_i}{\Delta x_i}\right)^3 \tag{22}$$

By Remark 1 the filtering strategy is the following:

- the input data s_i^0 are first filtered in the forward direction as suggested by the difference equation in (20) to get p_i.
- The output of this result p_i is then filtered in the backward direction according to the difference equation corresponding to backward equation in (21) in order to get s_i.

To complete the statements in (20) and (21) we fix the following heuristic initial conditions for the forward and backward procedures:

forward conditions	backward conditions
$p_1 = \beta_1 s_1^0$	$s_m = \beta_m p_m$
$p_2 = \beta_2 s_2^0 + \alpha_{2,1} p_1$	$s_{m-1} = \beta_{m-1} p_{m-1} + \alpha_{m-1,1} s_m$
$p_3 = \beta_3 s_3^0 + \alpha_{3,1} p_2 + \alpha_{3,2} p_1$	$s_{m-2} = \beta_{m-2} p_{m-2} + \alpha_{m-2,1} s_{m-1} + \alpha_{m-2,2} s_m$

(23)

Now we give some remarks on the accuracy and on the computational cost of an RF strategy.

Remark 2. For an arbitrary input distribution s_i^0, a measure for accuracy of an RF is given by the following inequality:

$$\|\epsilon_{s_i}\|_2 \leq \|\epsilon_{h_i}\|_2 \left\|s_i^0\right\|_2 \tag{24}$$

where:

- $\|\epsilon_{s_i}\|_2$ is the Euclidean norm of the difference between the discrete convolution $s_i^* = g_i \otimes s_i^0$ (with g_i normalized Gaussian function) and the function s_i, obtained by the RF applied to s_i^0.
- $\|\epsilon_{h_i}\|_2$ is the Euclidean norm of the difference between the Gaussian g_i and the function h_i (called *impulse response*), obtained by an RF applied to Dirac function;
- $\|s_i^0\|_2$ is the Euclidean norm of the input function s_i^0.

Proof. The proof is shown in Appendix A. □

By Remark 2 we observe that the approximation error $\|\epsilon_{s_i}\|_2$ of s_i^*, is smaller than arbitrary $\epsilon > 0$ if and only if $\|\epsilon_{h_i}\|_2 < \epsilon/\|s^0\|_2$. Then to get a good approximation of the Gaussian convolution s_i^*, it is necessary that the RF determines a good approximation h_i of Gaussian function g_i. Note that an accurate representation of the Gaussian function is especially required when velocities fields are assimilated or corrected by the data assimilation system. A rough approximation of the Gaussian leads to non-conservative quantities that might shock the subsequent forecast initialization. For instance, Purser et al. [23] provide an exemplification of that by comparing the Laplacians applied to different recursive filters, suggesting that only a fourth-order RF (or alternatively a 4-iteration first-order RF) is able to lead to an isotropic field.

It is interesting to highlight some practical considerations about the convergence, the accuracy on the boundaries and the inhomogeneous property of the RFs considered. We start to consider the convergence, choosing a one-dimensional grid of $m = 300$ points, a constant correlation radius $R = 12\,000$ m and a constant grid space $\Delta x = 6000$ m. In Fig. 1 we have the impulse response h_i, obtained by the 1st-RF and 3rd-RF applied to the unit impulse[3] in $x_0 = 0$, to reconstruct a Gaussian function with non-dimensional length-scale $\sigma = R/\Delta x$ and mean $\mu = 0$. In the left panel of Fig. 1 we observe the slow convergence of the 1st-RF that needs a high number of iterations to reach a good approximation of Gaussian function g_i. In the right panel of Fig. 1, we show the same with the 3rd-RF. For this case, it is needed just one iteration to obtain an accurate approximation h_i of the Gaussian function g_i.

[3] Value 1 in x_0 and 0 otherwise.

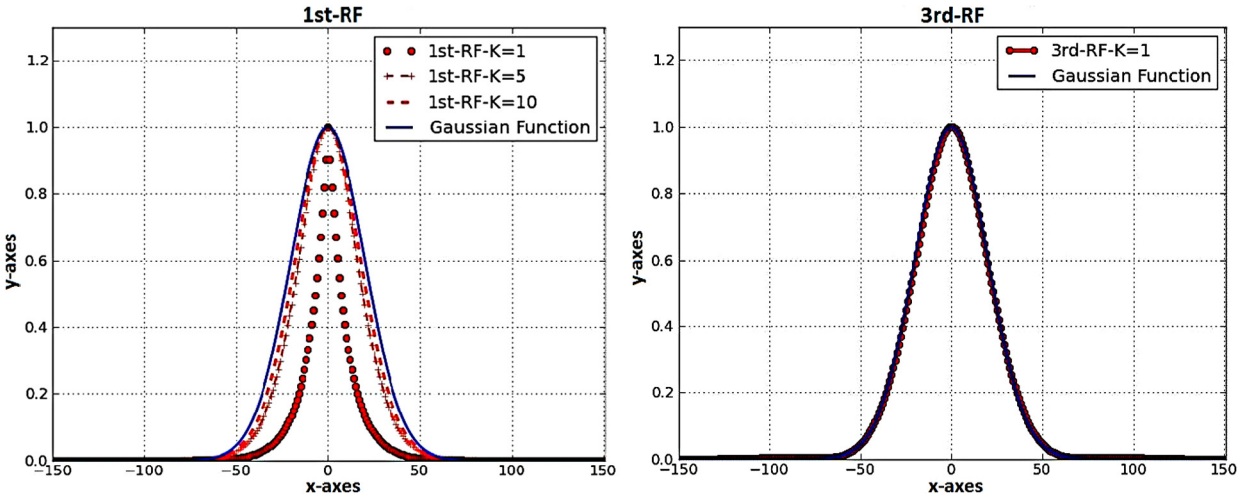

Fig. 1. Left – the impulse response h_i (red) resulting from the application of Eqs. (14) and (16) for $K = 1, 5, 10$ to the unit impulse in $x_0 = 0$ and the true Gaussian function g_i (blue) with non-dimensional length-scale $\sigma = R/\Delta x$ and mean $\mu = 0$. Right – the impulse response h_i (red) resulting from the application of Eqs. (30) and (31) for $K = 1$ to the unit impulse in $x_0 = 0$ and the true Gaussian function g_i (blue) with non-dimensional length-scale $\sigma = R/\Delta x$ and mean $\mu = 0$. (For interpretation of the references to color in this figure legend, the reader is referred to the web version of this article.)

In order to understand how RFs approximate the discrete Gaussian convolution also in presence of the boundaries as in a 3D-VAR ocean data assimilation system, it is useful to represent them in terms of matrix formulation. As explained in Purser et al. [23], Dahlquist and Bjorck [7], the computing of the convolution **s** with K iterations of a n-order recursive filter is equivalent to formally inverting a linear system. In particular, the convolution vector **s** is given by:

$$\mathbf{s} = (\mathbf{LU})^{-K}\mathbf{s}^0, \tag{25}$$

where matrices **L** and **U** are respectively lower and upper band triangular matrix with nonzero entries of the following form

$$U_{i,i} = L_{i,i} = \frac{1}{\beta_i}, \qquad L_{i,i-j} = U_{i,i+j} = -\frac{\alpha_{i,j}}{\beta_i}, \quad j \in [1, n] \tag{26}$$

and zero otherwise. It results that a direct expression of $(\mathbf{LU})^{-K}$ could be obtained, for $n = 1$ using the coefficients of the 1st-RF and for $n = 3$ using those of the 3rd-RF by means of the formulas in (26). In these terms, in the Fig. 2, as in Cuomo et al. [6], we show some features of numerical discrete operators. In particular, **V** represents the discrete convolution operator, **1st-RF-K=1** the first order filter with 1 iteration operator, **1st-RF-K=5** the first order filter with 5 iterations operator and, finally, the **3rd-RF**, the third order filter with 1 iteration operator. In Fig. 2, are highlighted some qualitative remarks in the hypothesis of homogeneous condition $\sigma_i = \sigma = 20$. **1st-RF-K=1** (Fig. 2 on the top-right) is a poor approximation of **V** (Fig. 2 on the top-left). Conversely, the operator **1st-RF-K=5** (Fig. 2 on the bottom-left) is closer to **V**, except in the top left and bottom right corners, as also for **3rd-RF** (Fig. 2 on the bottom-right), except this time only in bottom right corner. We underline that while for a 1st-RF the corners error approximation is presented in the top left and bottom right corners, instead for the proposed 3rd-RF this problem is only for the bottom right corner. These dissimilarities in the edges, by a numerical point of view, give some kind of artifacts in the computed convolutions **s**.

Hence RFs suffer mostly at the boundaries and those edge effects can decrease the accuracy of iterative solver used to minimize the cost function in (6) as it also shown in detail by Cuomo et al. [6]. Then one of major benefits of an RFs of high order as the 3rd-RF is that it needs only to pose suitable boundary conditions on right of the discrete domain; while a 1st-RF needs to put border conditions on both sides. The strategy used in OceanVar is to extend the grid over land in each iteration of the RFs by adding several imaginary sea points [10]. If the number of imaginary points is sufficiently large, the 1st-RF and 3rd-RF does not transfer the information across land and the backward process does not cause significant amplitude and phase (geometric position) distortion for all points near the boundaries. The drawback of this strategy is that **1st-RF-K=1, 5** and **3rd-RF** operators extend their size, increasing also the computational complexity, but the edge effects are transported on the lands. For the discussion related to Fig. 2, we underline that the 3rd-RF needs to extend the grid only on a one side with respect to 1st-RF that needs to extend the domain on the both sides. In the left panel of Fig. 3, we show how the RFs works very badly when the unit impulse is placed very close the boundaries ($x_0 = 140$) using a length-scale $\sigma = 20$ and grid size $m = 300$. Instead in the right panel of Fig. 3 we report how the RFs return to work very well with an extended grid of $3\sigma + x_0 - \frac{m}{2}$ (about 20% of the grid size m) on the right side of the domain by means of imaginary sea points.

In the last of our practical considerations we underline that the mathematical approach of both RFs is essentially based on the spatially homogeneous and isotropic Gaussian RFs [23,31] and due the different length-scales in the realistic applications of OceanVar, we just consider a punctuality scaling of σ as reported in Eqs. (19) for the 1st-RF and (22) for

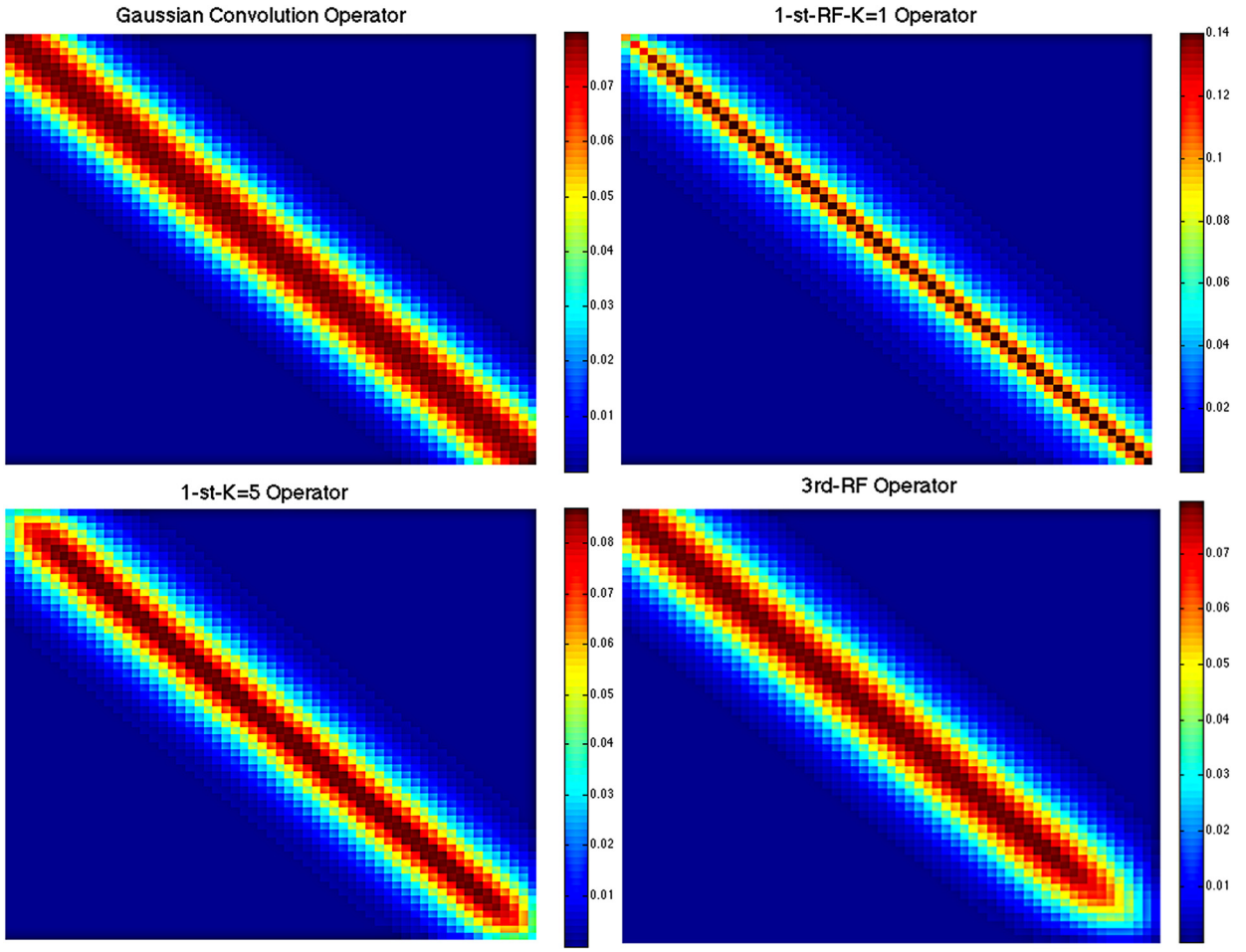

Fig. 2. Top-left. Discrete Gaussian convolution operator **V**. Top-right. **1st-RF-K=1** operator. Bottom-left. **1st-RF-K=1** operator. Bottom-right. **3rd-RF** operator.

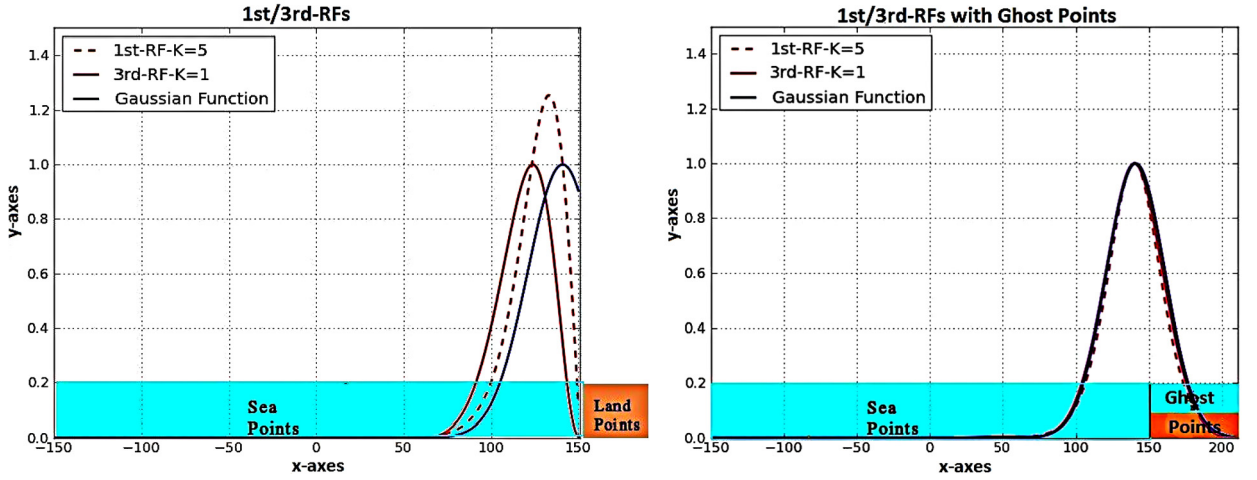

Fig. 3. Left – the red-dashed and red-line are the impulse responses resulting from the application of the 1st-RF-K=5 and 3rd-RF applied to the unit impulse on the sea points near the border (in $x_0 = 140$). The blue-line is a Gaussian function with non-dimensional length-scale $\sigma = 20$ and mean $\mu = 140$. Right – the red-dashed and red-line are the impulse responses resulting from the application of the 1st-RF-K=5 and 3rd-RF to the unit impulse (in $x_0 = 140$) on an extended grid of about 50 ghost (imaginary) sea points on the land. The blue-line is a Gaussian function with non-dimensional length-scale $\sigma = 20$ and mean $\mu = 140$. (For interpretation of the references to color in this figure legend, the reader is referred to the web version of this article.)

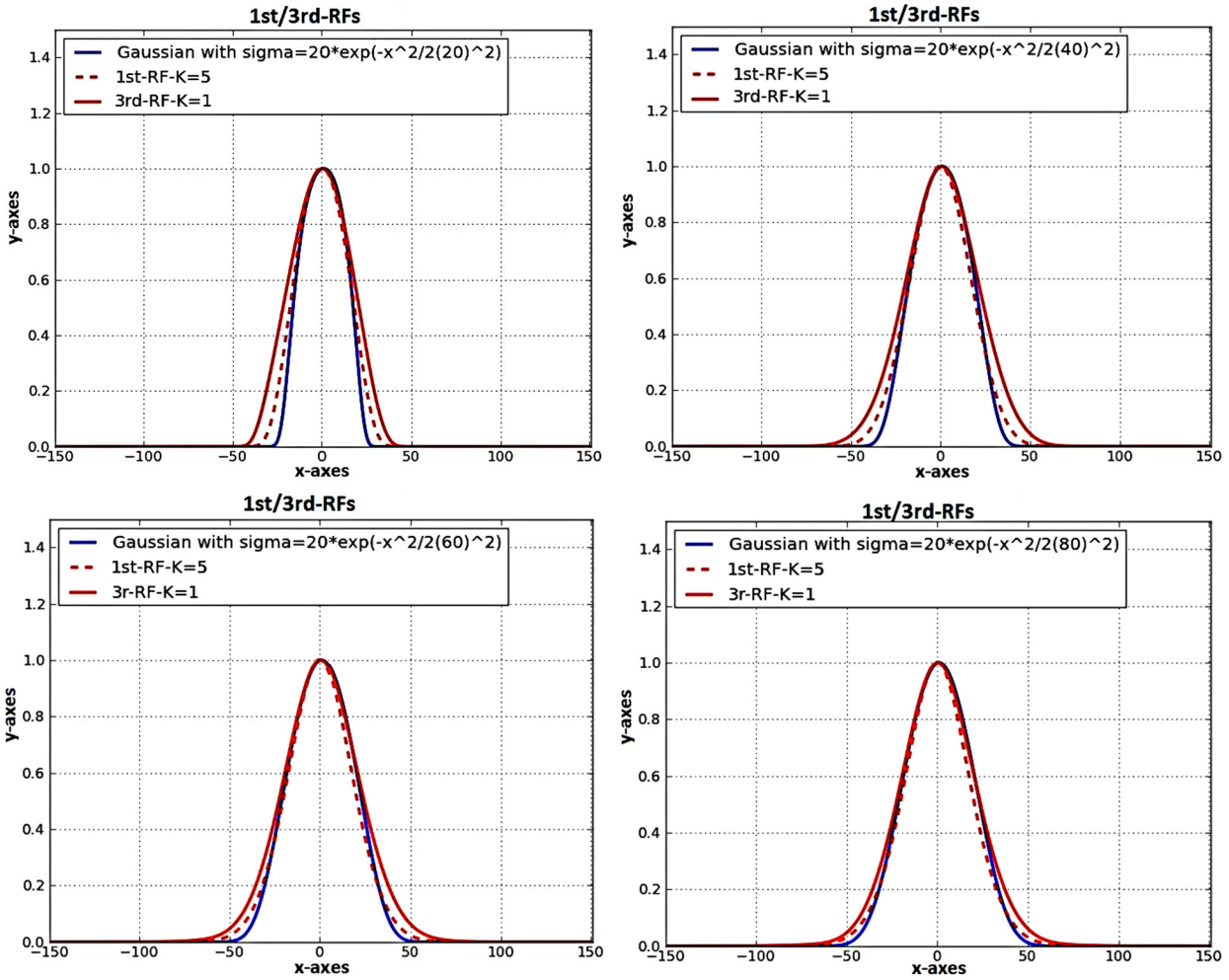

Fig. 4. The red-dashed and red-line are the impulse responses resulting from the application of the 1st-RF-K=5 and 3rd-RF to the unit impulse in $x_0 = 0$ and blue-line is a Gaussian function with a non-dimensional length-scale $\sigma(x) = Ae^{-x^2/2(\sigma_l)^2}$ with $\sigma_l = 20$ (top-left), $\sigma_l = 40$ (top-right), $\sigma_l = 60$ (bottom-left), $\sigma_l = 80$ (bottom-right) and mean $\mu = 0$. (For interpretation of the references to color in this figure legend, the reader is referred to the web version of this article.)

the 3rd-RF. We show, by means numerical experiments, here and in Section 5 (OceanVar in Global Implementation) that this way to consider different length-scales still retains the smooth properties of the 1st/3rd-RF if the $\sigma(x)$-variations are globally not very strong. In Fig. 4, we reported how 1st-RF-K=5 and 3rd-RF approximate a Gaussian function, of mean $\mu = 0$ and $\sigma(x) = Ae^{-x^2/2(\sigma_l)^2}$ i.e. a length-scale still Gaussian with $A = 20$ and $\sigma_l = 20, 40, 60$ and 80, on a domain of $m = 300$ points. By Fig. 4, we observe that both RFs tend to improve the approximation of the Gaussian function when its length-scale variations become smaller.

About the computational cost of RF we consider the following Remark 3.

Remark 3. The computational time of an n-th order accuracy RF is given by the following formula:

$$T(n, K, m) \approx 2(2n+1)mKt_{calc}, \tag{27}$$

where t_{calc} is the time for a floating point operation.

It immediately follows that the time complexity of the 1st-RF is:

$$T(1, K, m) \approx 6mKt_{calc} \tag{28}$$

Unfortunately, the 1st-RF needs a high step number K to determine a good approximation of the convolution function. We underline that this is a major obstacle in the OceanVar framework since the RF iterations are expensive from a computational point of view for real applications. Although the 3rd-RF complexity is

$$T(3, K, m) \approx 14mKt_{calc} \tag{29}$$

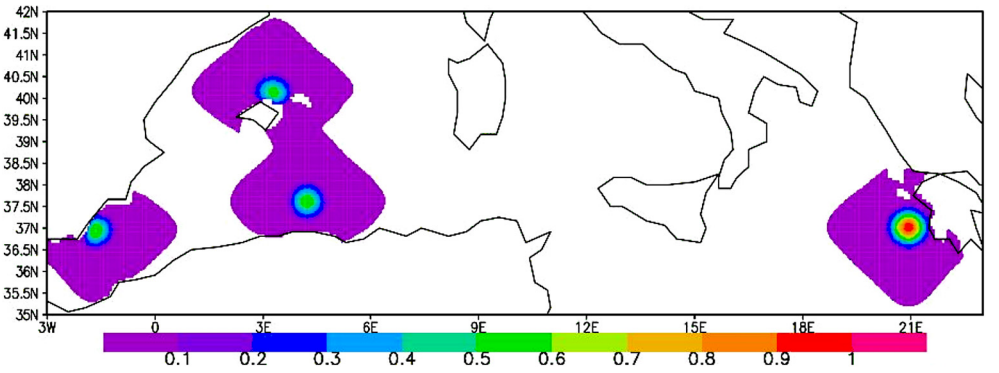

Fig. 5. Analysis increments of temperature at 300 m of depth for the Mediterranean Sea configuration using 3rd-RF.

we have good approximation of the convolution kernel with just one iteration. Note that by comparing the time complexities given by (28) and (29) it follows that the theoretical computational time of the 1st-RF is less than that of the 3rd-RF only if 1 or 2 iterations are used, which however provides a very inaccurate approximation of the Gaussian function.

In the next section, the benefits on the overall simulation scheme obtained by introducing a new 3rd order filter in the OceanVar software are confirmed by numerical experimentation.

4. Experimental results of OceanVar using 1st-RF and 3rd-RF in the Mediterranean Sea implementation

In this section we test the OceanVar set-up in Mediterranean Sea with the 1st-RF and 3rd-RF from a numerical point of view. Both 1st-RF and 3rd-RF allow us to use different filtering scales as we showed in Section 3 but in this configuration we fix a constant length-scale. This set-up follows the configuration of Dobricic and Pinardi [10], but the horizontal resolution is two times higher. In particular, the model has 72 horizontal levels, and the horizontal resolution is about 3.5 km in the latitudinal direction and between 3 km and 2.5 km in the longitudinal direction with a horizontal grid of $(1,742,506)$ points. The Mediterranean Sea has a relatively large variability of the bathymetry, with both deep ocean basins, like the Ionian Sea, the Levantine and the Western Mediterranean, and extended narrow shelves.

In this configuration we apply the 1st-RF and the 3rd-RF with the assimilation of only Argo floats profiles [22]. Here we compare (as also in the next experiments in Global Ocean but with different length-scales) accuracy, computational time (for 1 iteration of the minimizer) and the memory usage in the Mediterranean Sea. The numerical tests are carried out on a parallel IBM cluster (with 30 IBM P575 nodes, 960 cores Power6 4.7 GHz, Infiniband 4x DDR interconnection, Operating system AIX v.5.3).

In the following we start by comparing the accuracy of horizontal covariances in temperature by means of the two different RFs.

In Fig. 5, we illustrate analysis increment obtained using only one iteration of 3rd-RF on the Mediterranean Sea, for the temperature at 300 m, assuming isotropic and Gaussian spatial correlations by means of a constant correlation radius ($R = 15\,000$ m). The impression in Fig. 5, is that the 3rd-RF reconstructs quite successfully the horizontal covariances in just one iteration. The long range correlation shows more a diamond-like shape but the inner part, the most intense part of the field, has the right shape and amplitude. Moreover we underline that the 3rd-RF models the horizontal covariances near the coasts using the same number of the imaginary sea points used for the 1st-RF [10] because the approximate Gaussian functions built by both the RFs have the same length-scale.

Then we compute the horizontal temperature covariances at the same depth by means of the 1st-RF using $\mathrm{K} = 1$ iteration (1st-RF-K=1) in Fig. 6(a), 1st-RF, $\mathrm{K} = 5$ iterations (1st-RF-K=5) in Fig. 6(b) and 1st-RF, $\mathrm{K} = 10$ iterations (1st-RF-K=10) in Fig. 6(c). We can note that only with the 1st-RF $\mathrm{K} = 10$ (Fig. 6(c)) the horizontal covariances become isotropic and Gaussian.

Fig. 7 shows the absolute differences between the analyzed temperature fields computed by the 1st-RF-K=1 and the 3rd-RF (Fig. 7(a)), the 1st-RF-K=5 and the 3rd-RF (Fig. 7(b)) and the 1st-RF-K=10 and the 3rd-RF (Fig. 7(c)). Observing the maximum values of the differences in the three cases reported in Fig. 7 on the color-bars, it is evident that the same accuracy of the 3rd-RF can be achieved only with a large number of iterations of the other one. Qualitatively the results for salinity are the same as for temperature and hence we do not show them. At the last we want to underline that, in our numerical experiments, we used $K = 1, 5, 10$ to compare 1st-RF respect with 3rd-RF, but any k-value less of 5 for 1st-RF is not enough for the convergence of L-BFGS, although more convenient from a computational point of view. Hence the choice of a more accurate filter as 3rd-RF.

4.1. Performance results in Mediterranean Sea implementation

In the previous section we show that the use of a more accurate RF needs less iterations in order to obtain isotropic and Gaussian spatial horizontal covariances.

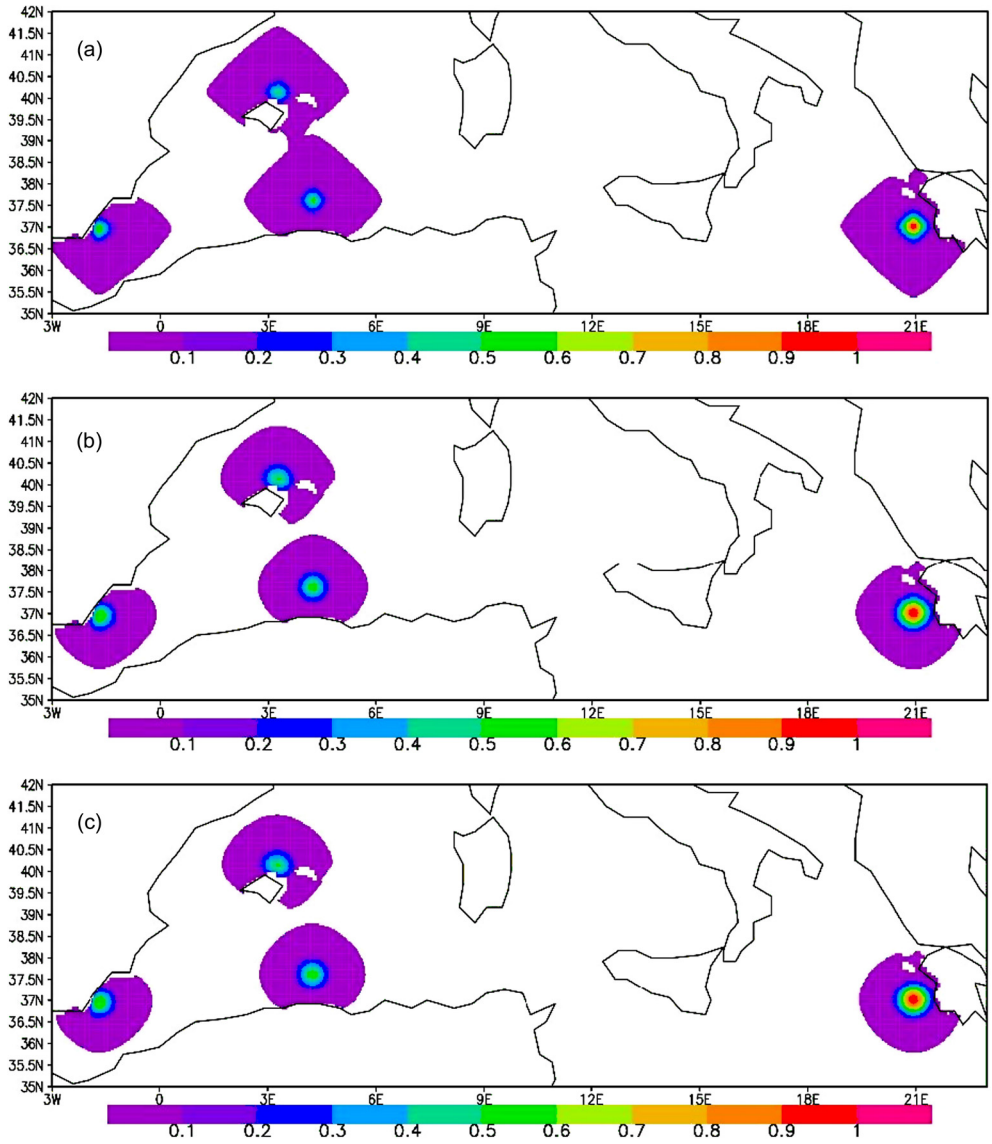

Fig. 6. Analysis increments of temperature at 300 m of depth for the Mediterranean Sea configuration using 1st-RF-K=1 (a), 1st-RF-K=5 (b) and 1st-RF-K=10 (c).

In this subsection we report the benefits and disadvantages of the 3rd-RF from a computational point of view. In particular here we give some information on the execution time and the memory usage in the parallel version of the 1st-RF and 3rd-RF of Oceanvar in Mediterranean Sea configuration.

The parallel implementation of the RF in Oceanvar uses communication strategies based on the pipeline method (e.g. [2]), because RF is a typical algorithm with flow dependences, where each iteration has to be strictly executed in a pre-fixed order. OceanVar in Mediterranean Sea configuration implements the pipeline method for the RF by using a column–row-wise block distribution of processors and blocking `mpi-send` and `mpi-receive` communication functions to transfer the boundary conditions. All the other operators in OceanVar (vertical EOFs, Vv, barotropic operator, Vn, velocities operator, Vuv, and divergence damping filter, Vd), along with the computations in observation space (misfits update, etc.) follow a Cartesian domain decomposition. The parallel implementation is also completely independent from that of the ocean model used for the forecasts. We modify OceanVar by substituting the 1st-RF with the 3rd-RF, without modifying the pipeline method.

As 3rd-RF needs only one iteration, it requires a smaller number of mpi-communications. This results in a sensible reduction in the latency in the communications. However 3rd-RF has to transfer a larger amount of data on each iteration. For example in the case of 1st-RF, in the forward filtering, the left processor sends only data on its last column to the right processor while in the case of 3rd-RF, the left processor sends data on its last three columns to the right processor.

Fig. 8 shows the execution time in seconds and the memory usage in Gbyte of the OceanVar with 1st-RF-K=1, 1st-RF-K=5, 1st-RF-K=10 and 3rd-RF on the IBM cluster using 64 processors. In particular we report the OceanVar and the

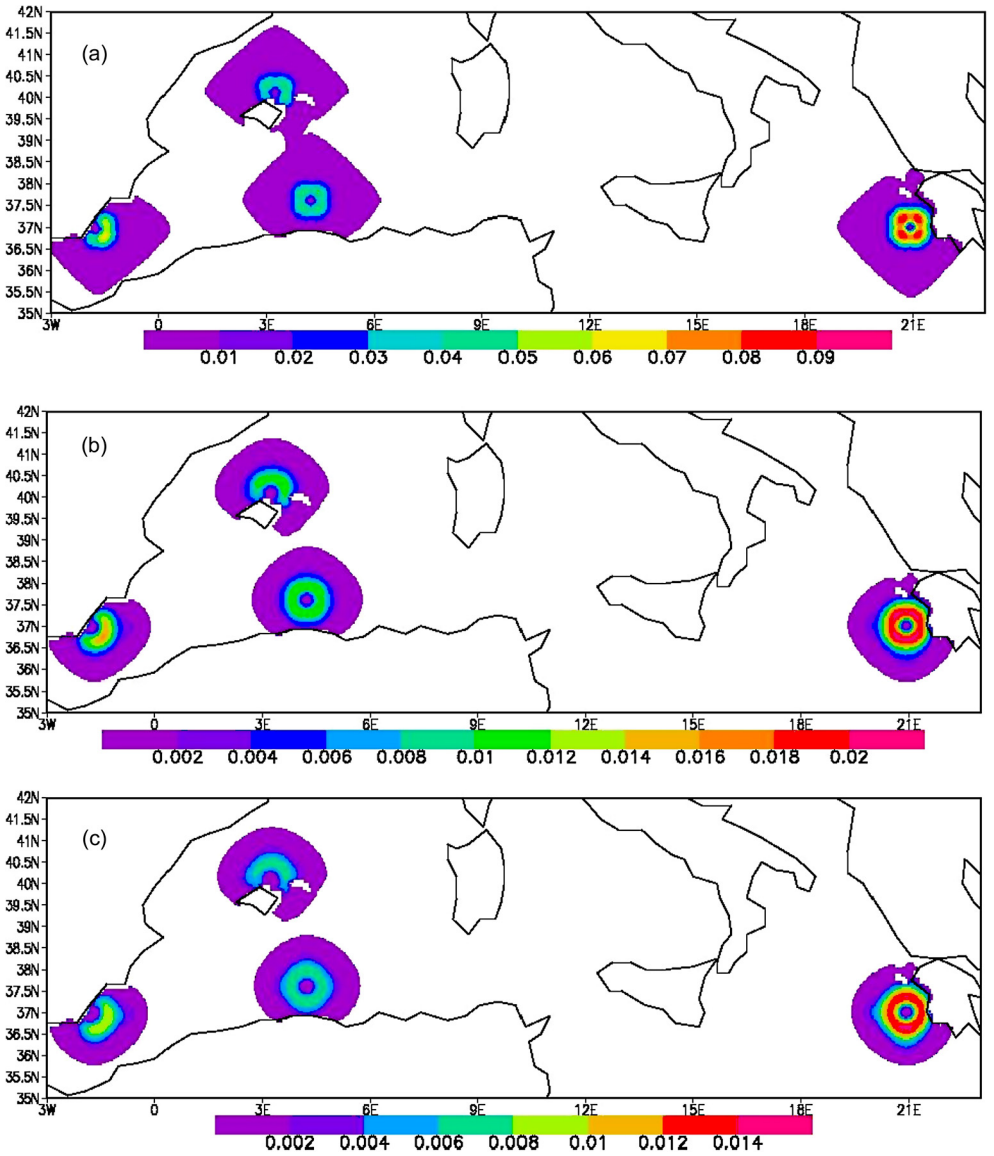

Fig. 7. Absolute differences for the temperature at 300 m of depth for the Mediterranean Sea configuration between 1st-RF-K=1 and 3rd-RF (a), 1st-RF-K=5 and 3rd-RF (b), 1st-RF-K=10 and 3rd-RF (c). (For interpretation of the references to color in this figure, the reader is referred to the web version of this article.)

RF wall clock times. To estimate the RF times in the software we synchronize all the processes in our mpi-communicator by using MPI-Barrier, before and after the implementation of RF.

Fig. 8 shows that Oceanvar with the 3rd-RF gives the best results in terms of the execution time if we consider the accuracy on the horizontal covariances discussed in the previous section. The 3rd-RF compared to the 1st-RF-K=5 and the 1st-RF-K=10 reduces the wall clock time of the software respectively of about 27% and 48%. The execution time is reduced because the new RF decreases the sequential time of each process in the mpi-communicator and needs only one `mpi-send` and `mpi-receive` communication for each process. The 3rd-RF algorithm uses twice as much memory than 1st-RF, because it has twice the number of filter coefficients. However, this did not represent a problem on our cluster because the maximum memory allowed was about 250 Gb.

5. Experimental results of OceanVar using 1st-RF and 3rd-RF in a global implementation

In this section, we describe experimental results of the 3rd-RF in a Global Ocean implementation of OceanVar that follows Storto et al. [27]. The model resolution is about 1/4 degree and the horizontal grid is tripolar, as described by Madec and Imbard [17]. This configuration of the model is used at CMCC for global ocean reanalysis applications [13]. The model

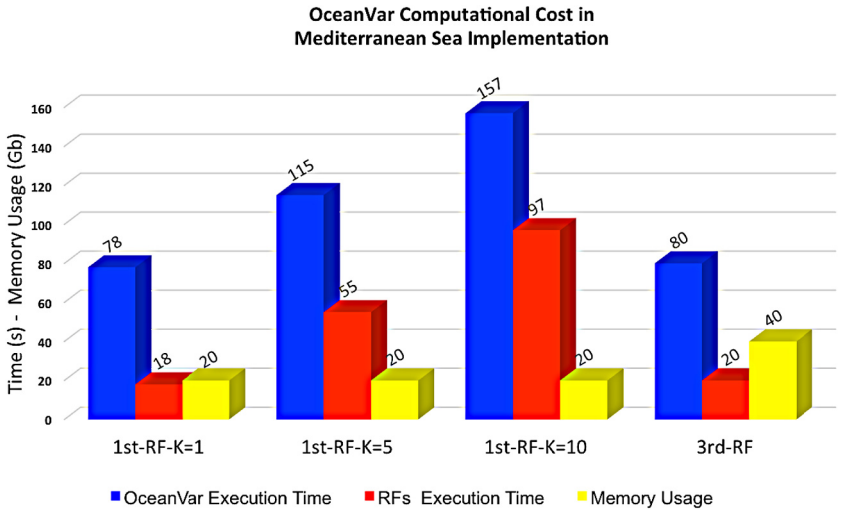

Fig. 8. Performance results (execution time and memory usage) on IBM Cluster (64 CPUs) for the recursive filter tests within the Mediterranean Sea implementation of OceanVar.

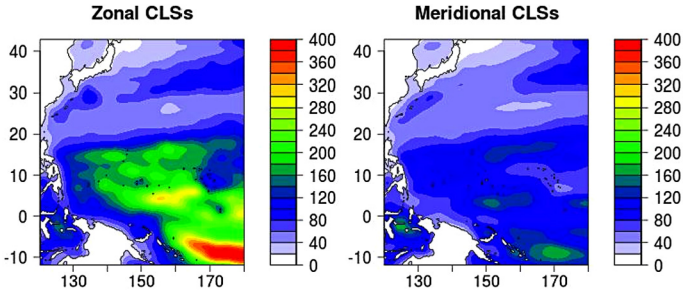

Fig. 9. Zonal (left) and meridional (right) correlation length-scales for temperature at 100 m of depth for the Western Pacific Area.

has 50 vertical depth levels. The three-dimensional model grid consists of 73 614 100 grid-points. The comparison between the 1st-RF and the 3rd-RF is here carried out for a realistic case study, where all in-situ observations of temperature and salinity from Expendable bathythermographs (XBTs), Conductivity, Temperature, Depth (CTDs) Sensors, Argo floats and Tropical mooring arrays are assimilated. The observational profiles are collected, quality-checked and distributed by Coriolis [5]. The global application of the recursive filter accounts for spatially varying and season-dependent correlation length-scales (CLSs), unlike the Mediterranean Sea implementation. Correlation length-scales were calculated by applying the approximation given by Belo Pereira and Berre [3] to a dataset of monthly anomalies with respect to the monthly climatology, with inter-annual trends removed. The two panels of Fig. 9 shows an example of zonal and meridional temperature correlation length-scales at 100 m of depth, respectively, for the winter season in the Western Pacific. A low-pass filter applied to the correlation length-scales guarantees that they are smoothed enough and vary slowly in space, allowing their successive use in the recursive filter. Typically, areas characterized by strong variability (e.g. Kuroshio Extension) present shorter correlation length-scales of the order of less than 100 km that lead to very narrow corrections, while in the Tropics the length-scales are longer and may reach up to 350 km, thus broadening the 3DVAR corrections. Furthermore, at the Tropics, it is acknowledged that zonal correlations are longer than the meridional ones (e.g., [8]). The analysis increments from a 3DVAR applications that uses the 1st-RF with 1, 5 and 10 iterations and the 3rd-RF are shown in Fig. 10, with a zoom in the same area of Western Pacific Area as in Fig. 9, for the temperature at 100 m of depth. The figure also displays the differences between the 3rd-RF and the 1st-RF with either 1 or 10 iterations. The patterns of the increments are quite similar, although increments for the case of 1st-RF-K=1 are generally sharper in the case of both short (e.g. off Japan) or long (e.g. off Indonesian region) CLSs. The panels of the differences reveal also that the differences between 3rd-RF and the 1st-RF-K=10 are very small, suggesting once again that the same accuracy of the 3rd-RF can be achieved only with a large number of iterations for the first order recursive filter.

5.1. Performance results in global implementation

In this subsection we present the performance results of the 3rd-RF with respect to the 1st-RF for the Global Ocean case study. OceanVar is run on a parallel IBM cluster, each of the 482 nodes with two eight-core Intel Xeon processors. We use

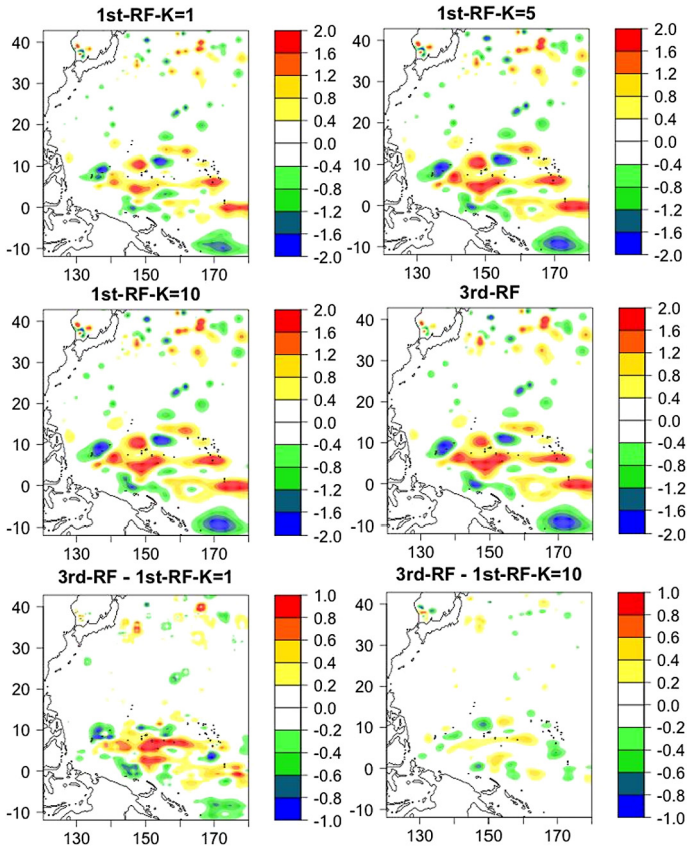

Fig. 10. Analysis increments of temperature at 100 m of depth for the Western Pacific for different configurations of the recursive filter (first two rows of panels). Differences of 100 m temperature analysis increments between 3rd-RF and 1st-RF-K=1 and between 3rd-RF and 1st-RF-K=10 (bottom panels).

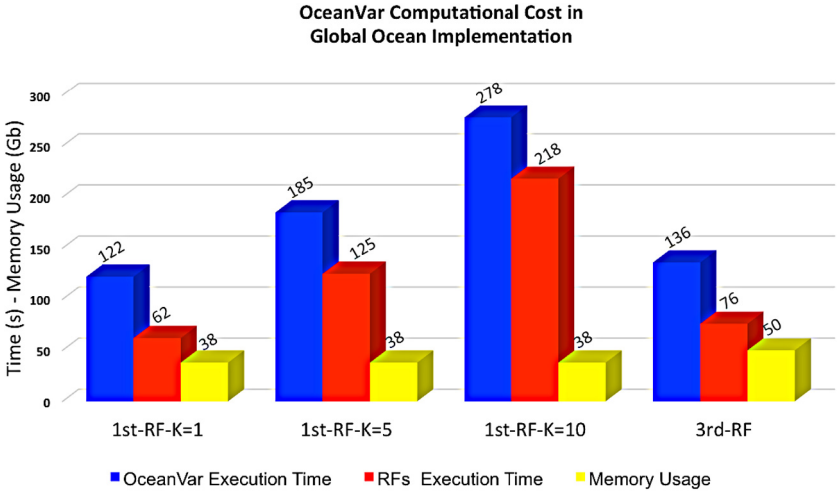

Fig. 11. Performance results (execution time and memory usage) for the recursive filter tests within the Global Ocean implementation of OceanVar.

a cluster different from the one previously introduced for the Mediterranean Sea configuration, in an attempt of presenting performance results also in different computing environments. The global ocean implementation of OceanVar has a parallel implementation that differs from the pipeline method previously presented: it exploits hybrid MPI-OpenMP parallelism, where OpenMP acts over the vertical level loops while MPI over the horizontal grid. This strategy has the advantage of limiting the MPI communication when exploiting the same number of cores, with the shortcoming of being not very flexible (due to the limitations of the cores-per-node number of threads for the OpenMP vertical parallelism). We have used 5 nodes for our tests: 5 MPI processes, 16 threads for a total of 80 cores used. Results are summarized in Fig. 11, when the number

of iterations of the 3DVAR minimizer is fixed to 30, as in realistic applications. Generally, relative performances of the two recursive filters are comparable with those of the Mediterranean Sea implementation. 3rd-RF reduces the total wall clock time of OceanVar by 28% and 51% with respect to 1st-RF-K=5 and 1st-RF-K=10, respectively. This reduction increases up to 42% and 65% if we consider only the recursive filter routines. On the other hand, the total memory usage increases from 36.4 Gb (7.3 Gb per node) to 47.6 Gb (9.5 Gb per node), i.e. by 30%. Thus, the third order recursive filter is able to significantly reduce the execution time at the price of an affordable increase of memory usage.

6. Conclusions

In this paper we describe the development and implementation of a revised scheme to compute the horizontal covariances of the temperature and the salinity in an oceanographic variational scheme.

The existing recursive filter (RF) of the first order (1st-RF) is replaced with a recursive filter of the third order (3rd-RF). Numerical experiments in Mediterranean Sea and Global Ocean demonstrated that a 3rd-RF can significantly reduce the total computational time of the data assimilation scheme maintaining the same level of accuracy.

In addition, we provide the full theoretical development of the new filter, based on the study by Young and Van Vliet [31] and Van Vliet et al. [28], who formulated the filter in the context of signal processing. We adapt it for a 3D-VAR oceanographic scheme with the detailed description of the process to obtain the 3rd-RF coefficients for different length-scales.

Our implementation is different to that by Purser et al. [23], since we have applied a different mathematical methodology to compute the filter coefficients. The new RF is faster than the previous one because it requires only one iteration to compute the horizontal covariances. Therefore, we may assume that it will be faster than other first order accurate methods that need several iterations like the one described by Mirouze and Weaver [18]. This hypothesis is tested with the pipeline method of Mediterranean Sea implementation and hybrid MPI-OpenMPI parallelization strategy of the Global Ocean configuration presented in the previous sections. By applying some other parallelization strategy the relative performance of the new filter may differ. However, we believe that other parallelization strategies are overall much less efficient than those presented. A useful suggestion to improve the performance of variational methods in data assimilations problems could be the use of accelerated schemes for graphic processor units (GPUs) as in [11,12]. The future improvement of the 3rd-RF scheme in OceanVar will be the implementation of different mathematical boundary conditions at the coasts and a formulation of 3rd-RF for spatially anisotropic covariances.

Acknowledgements

The research leading to these results has received funding from the Italian Ministry of Education, University and Research and the Italian Ministry of Environment, Land and Sea under the GEMINA and Next Data projects. We also thank the researchers Ardelio Galletti and Livia Marcellino of the University of Naples “Parthenope”, Department of Science and Technology, Italy, for useful discussions. Finally we specially thank the anonymous referees for the work improvement.

Appendix A

Theorem 1. *For each i-th grid point of a finite one-dimensional grid with correlation radius R and grid spacing Δx, a normalized, spatially homogeneous and isotropic 3rd-RF is given by:*

$$p_i = \beta s_i^0 + \alpha_1 p_{i-1} + \alpha_2 p_{i-2} + \alpha_3 p_{i-3} \quad i = 4, m \ : +1 \tag{30}$$

$$s_i = \beta p_i + \alpha_1 s_{i+1} + \alpha_2 s_{i+2} + \alpha_3 s_{i+3}. \quad i = m-3, 1 \ : -1. \tag{31}$$

where the function s_i^0 is the input distribution, $\alpha_1 = a_1/a_0$, $\alpha_2 = a_2/a_0$, $\alpha_3 = a_3/a_0$ and $\beta = \sqrt[4]{2\pi\,(R/\Delta x)^2}(1 - (\alpha_1 + \alpha_2 + \alpha_3))$ are the filtering coefficients and:

$$a_0 = 3.738128 + 5.788982\left(\frac{R}{\Delta x}\right) + 3.382473\left(\frac{R}{\Delta x}\right)^2 + 1.\left(\frac{R}{\Delta x}\right)^3$$

$$a_1 = 5.788982\left(\frac{R}{\Delta x}\right) + 6.764946\left(\frac{R}{\Delta x}\right)^2 + 3.\left(\frac{R}{\Delta x}\right)^3$$

$$a_2 = -3.382473\left(\frac{R}{\Delta x}\right)^2 - 3.\left(\frac{R}{\Delta x}\right)^3$$

$$a_3 = 1.\left(\frac{R}{\Delta x}\right)^3$$

Proof. In order to obtain an efficient RF such that approximates the Gaussian convolution (as considered in [18]):

$$s(x) = g(x) \otimes s^0(x) = \int_{-\infty}^{+\infty} g(x-\tau)s^0(\tau)d\tau, \tag{32}$$

we apply the Fourier transformation to the equation in (32), where $g(x) = \exp(-\frac{x^2}{2\sigma^2})$ is the normalized Gaussian function of mean $\mu = 0$ and non-dimensional length-scale $\sigma = R/\Delta x$ associated to i-th grid point. Hence we obtain:

$$S(w) = G(w)S^0(w) \quad w \in \mathbb{R} \tag{33}$$

where $S(w), G(w)$ and $S^0(w)$ in (33) are respectively the Fourier transformations of the function $s(x)$, $g(x)$, and $s^0(x)$. For the Fourier transformation of $g(x)$, we have the well-known result:

$$G(w) = \sqrt{2\pi}\sigma e^{-\frac{(\sigma\omega)^2}{2}}. \tag{34}$$

Using a rational approximation of the Gaussian function in [1]:

$$\frac{1}{\sqrt{2\pi}}e^{-\frac{t^2}{2}} = \frac{1}{b_0 + b_2t^2 + b_4t^4 + b_6t^6} + \epsilon(t), \quad t \in \mathbb{R} \tag{35}$$

where $b_0 = 2.490895$, $b_2 = 1.466003$, $b_4 = -0.024393$, $b_6 = 0.178257$ and $\epsilon(t) < 2.7 * 10^{-3}$, then we can approximate the $G(w)$ function as:

$$G(w) \approx H_\sigma(w) = \frac{2\pi\sigma C^2}{b_0 + b_2(\sigma w)^2 + b_4(\sigma w)^4 + b_6(\sigma w)^6} \tag{36}$$

where C^2 is a square of a normalization constant that we will choose later. The absolute error $|\epsilon(w)|$ between $G(w)$ and $H_\sigma(w)$ is less than $5.4\pi\sigma \times 10^{-3}$. Moreover we can rewrite the $H_\sigma(\omega)$ as a function in the complex field:

$$H_\sigma(s) = \frac{2\pi\sigma C^2}{b_0 - b_2(\sigma s)^2 + b_4(\sigma s)^4 - b_6(\sigma s)^6}, \quad \text{with } s = i\omega \in \mathbb{C} \tag{37}$$

Through the non-linear Newton Formula (e.g., [25]), we determine two real solutions $s = \pm 1.16680481/\sigma$ of the polynomial $b_0 - b_2(\sigma s)^2 + b_4(\sigma s)^4 - b_6(\sigma s)^6$. After we divide it by $((\sigma s)^2 - 1.6680481^2)$ and obtain a polynomial quotient that is the difference between a polynomial of the fourth degree and second one. Hence the rational polynomial $H_\sigma(s)$ can be decomposed in the following way:

$$H_\sigma(s) = H_{\sigma,b}(s)H_{\sigma,f}(s) \tag{38}$$

where

$$H_{\sigma,f}(s) = \frac{\sqrt{(2\pi\sigma)}C}{(1.166805 + \sigma s)(3.203730 + 2.215668\sigma s + (\sigma s)^2)} \tag{39}$$

$$H_{\sigma,b}(s) = \frac{\sqrt{(2\pi\sigma)}C}{(1.166805 - \sigma s)(3.203730 - 2.215668\sigma s + (\sigma s)^2)}. \tag{40}$$

Using standard approximations as the backward and forward differences for the $\mathcal{Z}$ transformation (e.g., [20]) to switch from continuous to discrete problem, we replace $s = 1 - z^{-1}$ in (39) and $s = z - 1$ in (40) as in Young and Van Vliet [31]. Hence we obtain:

$$H_{\sigma,f}(z^{-1}) = \frac{\sqrt{(2\pi\sigma)}C}{(1.166805 + \sigma(1 - z^{-1}))(3.203730 + 2.215668\sigma(1 - z^{-1}) + (\sigma(1 - z^{-1}))^2)}$$

$$H_{\sigma,b}(z) = \frac{\sqrt{(2\pi\sigma)}C}{(1.166805 - \sigma(z - 1))(3.203730 - 2.215668\sigma(z - 1) + (\sigma(z - 1))^2)}$$

Both previous equations can be rewritten respectively as standard polynomials in z^{-1} and z:

$$H_{\sigma,f}(z^{-1}) = \frac{\sqrt{(2\pi\sigma)}C}{(a_0 - a_1z^{-1} - a_2z^{-2} - a_3z^{-3})} \tag{41}$$

$$H_{\sigma,b}(z) = \frac{\sqrt{(2\pi\sigma)}C}{(a_0 - a_1z^1 - a_2z^2 - a_3z^3)}, \tag{42}$$

where we can determine the following coefficients for (41) and (42):

$$a_0 = \left(3.738128 + 5.788982\sigma + 3.382472\sigma^2 + 1.\sigma^3\right)$$
$$a_1 = \left(5.788824\sigma + 6.764946\sigma^2 + 3.\sigma^3\right)$$
$$a_2 = \left(-3.382472\sigma^2 - 3.\sigma^3\right)$$
$$a_3 = \left(1.\sigma^3\right) \tag{43}$$

The normalized constant C can be specified by using the constrain that the approximation Gaussian function $H_\sigma(\omega)$ must be $\sqrt{2\pi}\sigma$ for $\omega = 0$ (see Eqs. (34) and (36)) hence $H_{\sigma,f}(z^{-1}) = 1 \wedge H_{\sigma,b}(z) = \sqrt[4]{(2\pi\sigma^2)}$ for $z^{-1} = 1 \wedge z = 1$. It follows that:

$$C = \frac{(a_0 - (a_1 + a_2 + a_3))}{\sqrt[4]{(2\pi)}} \tag{44}$$

Place $P(z) = H_{\sigma,f}(z)S^0(z)$ and $S(z) = H_{\sigma,b}(z)P(z)$, we have:

$$H_{\sigma,f}(z) = \frac{P(z)}{S^0(z)} = \frac{\sqrt[4]{(2\pi\sigma^2)}(a_0 - (a_1 + a_2 + a_3))}{(a_0 - a_1 z^{-1} - a_2 z^{-2} - a_3 z^{-3})} \tag{45}$$

$$H_{\sigma,b}(z) = \frac{S(z)}{P(z)} = \frac{\sqrt[4]{(2\pi\sigma^2)}(a_0 - (a_1 + a_2 + a_3))}{(a_0 - a_1 z - a_2 z^2 - a_3 z^3)} \tag{46}$$

from which we obtain respectively:

$$\left(a_0 - a_1 z^{-1} - a_2 z^{-2} - a_3 z^{-3}\right)P(z) = \sqrt[4]{\left(2\pi\sigma^2\right)}\left(a_0 - (a_1 + a_2 + a_3)\right)S^0(z), \tag{47}$$

$$\left(a_0 - a_1 z^{-1} - a_2 z^{-2} - a_3 z^{-3}\right)S(z) = \sqrt[4]{\left(2\pi\sigma^2\right)}\left(a_0 - (a_1 + a_2 + a_3)\right)P(z). \tag{48}$$

Antitransforming, by means of the $\mathcal{Z}^{-1}$ transformation, Eqs. (47) and (48) and by the theorem of the delay (e.g., [20]), we obtain the following forward and backward finite difference equations:

$$p_i = \beta s_i^0 + \alpha_1 p_{i-1} + \alpha_2 p_{i-2} + \alpha_3 p_{i-3} \tag{49}$$

$$s_i = \beta p_i + \alpha_1 s_{i+1} + \alpha_2 s_{i+2} + \alpha_3 s_{i+3} \tag{50}$$

where the functions p_i and s_i are respectively the $\mathcal{Z}^{-1}$ transformations of $P(z)$ and $S(z)$ functions and the filtering coefficients are $\alpha_1 = a_1/a_0$, $\alpha_2 = a_2/a_0$, $\alpha_3 = a_3/a_0$ and $\beta = \sqrt[4]{(2\pi\sigma^2)}(1 - (\alpha_1 + \alpha_2 + \alpha_3))$. Remembering that $\sigma = R/\Delta x$ then from Eqs. (43), (49) and (50) and the values of the filtering coefficients α_1, α_2, α_3 and β, we obtain the thesis. □

Remark 2. For an arbitrary input distribution s_i^0, a measure for accuracy of an RF is given by the following inequality:

$$\|\epsilon_{s_i}\|_2 \le \|\epsilon_{h_i}\|_2 \left\|s_i^0\right\|_2 \tag{51}$$

where:

- $\|\epsilon_{s_i}\|_2$ is the Euclidean norm of the difference between the discrete convolution $s_i^* = g_i \otimes s_i^0$ (with g_i normalized Gaussian function) and the function s_i, obtained by the RF applied to s_i^0.
- $\|\epsilon_{h_i}\|_2$ is the Euclidean norm of the difference between the Gaussian g_i and the function h_i (called *impulse response*), obtained by an RF applied to Dirac function;
- $\|s_i^0\|_2$ is the Euclidean norm of the input function s_i^0.

Proof. The error in the output per sample when we substitute the true convolution s_i^* with an approximation s_i is given by

$$\epsilon_{s_i} = s_i^* - s_i = (g_i - h_i) \otimes s_i^0 = \varepsilon_{h_i} \otimes s_i^0. \tag{52}$$

Hence the following holds:

$$\|\epsilon_{s_i}\|_2 = \left\|\epsilon_{h_i} \otimes s_i^0\right\|_2 \tag{53}$$

and applying the Cauchy–Schwarz inequality to the right-hand side of Eq. (53), it gives the condition:

$$\|\epsilon_{s_i}\|_2 \le \|\epsilon_{h_i}\|_2 \left\|s_i^0\right\|_2 \qquad \square \tag{54}$$

References

[1] M. Abramowitz, I. Stegun, Handbook of Mathematical Functions, Dover, New York, 1965.
[2] Y. Aoyama, J. Nakano, RS/6000 SP: Practical MPI Programming, International Technical Support Organization IBM, 1999.
[3] M. Belo Pereira, L. Berre, The use of an ensemble approach to study the background-error covariances in a global NWP model, Mon. Weather Rev. 134 (2006) 2466–2489.
[4] R. Byrd, J. Nocedal, C. Zhu, A limited memory algorithm for bound constrained optimization, SIAM J. Sci. Comput. 16 (1995) 1190–1208.
[5] C. Cabanes, A. Grouazel, K. von Schuckmann, M. Hamon, V. Turpin, C. Coatanoan, F. Paris, S. Guinehut, C. Boone, N. Ferry, C. de Boyer Montégut, T. Carval, G. Reverdin, S. Pouliquen, P.-Y.L. Traon, The CORA dataset: validation and diagnostics of in-situ ocean temperature and salinity measurements, Ocean Sci. 9 (2013) 1–18.
[6] S. Cuomo, A. Galletti, L. Marcellino, R. Farina, An error estimate of Gaussian Recursive Filter in 3Dvar problem, in: Proceedings of the 2014 Federated Conference on Computer Science and Information Systems, in: Ann. Comput. Sci. Inf. Syst., vol. 2, IEEE, 2014.
[7] G. Dahlquist, A. Bjorck, Numerical Methods, Prentice Hall, 2014, 573 pp.
[8] J. Derber, A. Rosati, A global oceanic data assimilation system, J. Phys. Oceanogr. 19 (1989) 1333–1347.
[9] R. Deriche, Separable recursive filtering for efficient multi-scale edge detection, in: Proc. Internat. Workshop on Industrial Application of Machine Vision and Machine Vision and Machine Intelligence, Tokyo, 1987, pp. 18–23.
[10] S. Dobricic, N. Pinardi, An oceanographic three-dimensional variational data assimilation scheme, Ocean Model. 22 (2008) 89–105.
[11] R. Farina, S. Cuomo, P. De Michele, CUBLAS-CUDA implementation of PCG method of an ocean circulation model, in: ICNAAM 2011: International Conference on Numerical Analysis and Applied Mathematics, vol. 1389, no. 1, AIP Publishing, 2011.
[12] R. Farina, S. Cuomo, P. De Michele, F. Piccialli, A smart GPU implementation of an elliptic kernel for an ocean global circulation model, Appl. Math. Sci. 7 (61) (2013) 3007–3021.
[13] N. Ferry, B. Barnier, G. Garric, K. Haines, S. Masina, L. Parent, A. Storto, M. Valdivieso, S. Guinehut, S. Mulet, NEMO: the modeling engine of global ocean reanalyses, Mercator Ocean Q. Newsl. 46 (2012) 60–66.
[14] C. Hayden, R. Purser, Recursive filter objective analysis of meteorological fields: applications to NESDIS operational processing, J. Appl. Meteorol. 34 (1995) 3–15.
[15] A. Lorenc, Optimal nonlinear objective analysis, Q. J. R. Meteorol. Soc. 114 (1988) 205–240.
[16] A. Lorenc, Iterative analysis using covariance functions and filters, Q. J. R. Meteorol. Soc. 1 (118) (1992) 569–591.
[17] G. Madec, M. Imbard, A global ocean mesh to overcome the north pole singularity, Clim. Dyn. 12 (1996) 381–388.
[18] I. Mirouze, A. Weaver, Representation of correlation functions in variational assimilation using an implicit diffusion operator, Q. J. R. Meteorol. Soc. 136 (2010) 1421–1443.
[19] I.M. Navon, N. Daescu Dacian, Z. Liu, The impact of background error on incomplete observations for 4D-Var data assimilation with the FSU GSM, in: V.S. Sunderam, et al. (Eds.), Computational Science – ICCS 2005, in: LNCS, vol. 3515, Springer-Verlag, Heidelberg, 2005, pp. 837–844.
[20] A. Oppenheim, A. Willsky, S. Nawab, Signals and Systems, Prentice Hall, 1983.
[21] N. Pinardi, I. Allen, E. Demirov, P.D. Mey, G. Korres, A. Lascaratos, P.L. Traon, C. Maillard, G. Manzella, C. Tziavos, The Mediterranean ocean forecasting system: first phase of implementation, Ann. Geophys. 21 (21) (2010) 3–20.
[22] P. Poulain, R. Barbanti, J. Font, A. Cruzado, C. Millot, I. Gertman, A. Griffa, A. Molcard, V. Rupolo, S.L. Bras, L. Petit de la Villeon, MedArgo: a drifting profiler program in the Mediterranean Sea, Ocean Sci. 3 (2007) 379–395.
[23] R. Purser, W. Wu, D. Parish, N. Roberts, Numerical aspects of the application of recursive filters to variational statistical analysis. Part I: spatially homogeneous and isotropic covariances, Mon. Weather Rev. 131 (2003) 1536–1548.
[24] R. Purser, W. Wu, D. Parish, N. Roberts, Numerical aspects of the application of recursive filters to variational statistical analysis. Part II: spatially inhomogeneous and anisotropic general covariances, Mon. Weather Rev. 131 (2003).
[25] A. Quarteroni, R. Sacco, F. Saleri, Numerical Mathematics, Springer, 2007.
[26] J.L. Steward, I.M. Navon, M. Zupanski, N. Karmitsa, Impact of non-smooth observation operators on variational and sequential data assimilation for a limited-area shallow water equations model, Q. J. R. Meteorol. Soc. 138 (663) (January 2012) 323–339, Part B.
[27] A. Storto, S. Dobricic, S. Masina, P.D. Pietro, Assimilating along-track altimetric observations through local hydrostatic adjustments in a global ocean reanalysis system, Mon. Weather Rev. 139 (2011) 738–754.
[28] J. Van Vliet, I. Young, P. Verbee, Recursive Gaussian derivative filters, in: Proceedings of the Fourteenth International Conference on Pattern Recognition, vol. 1, 1998, pp. 509–514.
[29] A. Weaver, P. Courtier, Correlation modelling on the sphere using a generalized diffusion equation, Q. J. R. Meteorol. Soc. 127 (2001) 1815–1846.
[30] A. Weaver, J. Vialard, D. Anderson, Three- and four-dimensional variational assimilation with an ocean general circulation model of the tropical Pacific Ocean. Part 1: formulation, internal diagnostics and consistency checks, Mon. Weather Rev. 131 (2003) 1360–1378.
[31] L. Young, I. Van Vliet, Recursive Implementation of the Gaussian filter, Signal Process. 44 (1995) 139–151.